Rheological measurements of large particles in high shear rate flows

Erin Koos,[1] Esperanza Linares-Guerrero,[2] Melany L. Hunt,[2,a)]
and Christopher E. Brennen[2]
[1]*Institute for Mechanical Process Engineering and Mechanics, Karlsruhe Institute of Technology, 76131, Karlsruhe, Germany*
[2]*Mechanical Engineering, California Institute of Technology; MC 104-44; Pasadena, California 91125, USA*

(Received 10 October 2011; accepted 20 December 2011; published online 27 January 2012)

This paper presents experimental measurements of the rheological behavior of liquid-solid mixtures at moderate Stokes and Reynolds numbers. The experiments were performed in a coaxial rheometer that was designed to minimize the effects of secondary flows. By changing the shear rate, particle size, and liquid viscosity, the Reynolds numbers based on shear rate and particle diameter ranged from 20 to 800 (Stokes numbers from 3 to 90), which is higher than examined in earlier rheometric studies. Prior studies have suggested that as the shear rate is increased, particle-particle collisions also increase resulting in a shear stress that depends non-linearly on the shear rate. However, over the range of conditions that were examined in this study, the shear stress showed a linear dependence on the shear rate. Hence, the effective relative viscosity is independent of the Reynolds and Stokes numbers and a non-linear function of the solid fraction. The present work also includes a series of rough-wall experiments that show the relative effective viscosity is also independent of the shear rate and larger than in the smooth wall experiments. In addition, measurements were made of the near-wall particle velocities, which demonstrate the presence of slip at the wall for the smooth-walled experiments. The depletion layer thickness, a region next to the walls where the solid fraction decreases, was calculated based on these measurements. The relative effective viscosities in the current work are larger than found in low-Reynolds number suspension studies but are comparable with a few granular suspension studies from which the relative effective viscosities can be inferred. [doi:10.1063/1.3677687]

I. INTRODUCTION

Liquid-solid flows occur in a variety of fields ranging from mining operations and clogging of drilling wells to the erosion of the Martian landscape. Because of the collisional interactions, particulate flows are used to polish and cut metal in manufacturing practices and can cause deterioration of industrial components. To enable predictions of flow and transport of these two-phase mixtures, researchers need accurate models of the constitutive relations over a range of flow conditions. The current research focuses on flows in which the inertia of both the liquid and solid phases is significant.

Extensive research has been done on the rheology of non-inertial suspensions in the limit of vanishingly small Reynolds numbers, where Re is defined as $Re = \rho\dot{\gamma}d^2/\mu$, ρ and μ are the density and dynamic viscosity of the suspending liquid, $\dot{\gamma}$ is the shear rate, and d is the particle diameter.[1,2] For these flows (typically $d \ll 1$ mm and $Re \ll 10^{-2}$), the shear stress, τ, is equated to the shear rate and an effective viscosity, μ'. As found in many prior studies,[1,2] the effective viscosity is strongly dependent on the solid fraction, ϕ. For solid fractions greater than approximately 40%, the effective viscosity may also depend on the shear rate with the effective viscosity showing a shear thinning behavior at low shear rates and shear thickening at high shear rates.[2] Additionally,

a)Electronic mail: hunt@caltech.edu.

wall slip can influence the effective viscosity measurements and the conclusions from an experiment may be marred if the effect of slip is not considered.[3] Most multi-phase flows and complex fluids can exhibit slip at solid walls.[4] One way to counteract the wall slip is by using roughened rheometer surfaces.[5,6]

Fewer suspension studies have been conducted with grain sizes larger than a millimeter and at Reynolds numbers greater than one.[7–10] In these high Reynolds number flows, the inertia of one or both phases is important and collisions between the particles may occur; the flow may also transition to turbulence. The first experimental study exploring the transition to an inertial suspension flow was conducted by Bagnold[7,11] who made rheometric measurements using a small concentric cylinder device with an outer rotating wall. Using this device, he measured the shear and normal stresses for neutrally buoyant suspensions over a range of shear rates and particle concentrations. At low shear rates in the "macroviscous regime," the tangential stresses were linearly proportional to the dynamic viscosity of the liquid, the shear rate, and a function of solid fraction, $\tau \approx \mu\dot{\gamma}f_1(\phi)$. At larger shear rates, similar to the results found for non-inertial suspensions in the "grain-inertia regime," the stresses were independent of fluid viscosity and depended on the square of the shear rate, the square of the particle diameter, the particle density, and displayed a stronger dependence on the solid fraction ($\tau \approx \rho_p^2 d^2\dot{\gamma}^2 f_2(\phi)$). Bagnold distinguished the two regimes by defining a parameter, N, from the ratio of the scaling of the stresses, $N = \rho_p d^2\dot{\gamma}^2 f_1(\phi)/(\mu\dot{\gamma}f_2(\phi)) = \rho_p d^2\dot{\gamma}h(\phi)/\mu$, where $h(\phi)$ is a function that increases with solid fraction. The parameter, N, has been referred to as the Bagnold number, and according to Bagnold $N \approx 450$ marked the transition from the viscous regime to the inertial regime. Zeininger and Brennen found a similar transitional Bagnold number for their hopper flows experiments.[12] However, it is important to note that Bagnold's experiments involved neutrally buoyant particles so that the fluid and solid densities matched, $\rho_f = \rho_p$. In addition, Bagnold used only 1 mm deformable wax beads. Hence, in these experiments, only the shear rate and the fluid viscosities were varied; the density and the particle size were fixed.

The Bagnold work was followed by the high-Reynolds number studies by Savage and McKeon[8] in which the researchers made measurements of the shear stress in a concentric cylinder rheometer with a rotating inner cylinder. Using a neutrally buoyant liquid-solid suspension, they varied the particle size from 1 to 2 mm diameter and the roughness of the driving surfaces. Their results did not strictly follow the work of Bagnold. Although they found that shear stress varied with the square of the shear rate, they did not find a dependence on the square of the particle diameter. Their work suggested that the flow was governed not only by the length scale of the particles but also by the scale of the experimental apparatus.

Following that work, Prasad and Kytomaa[9] performed similar shear cell tests at high solid fractions using 3 mm particles that were denser than the surrounding fluid. Their results focused on the transition from a static bed to the viscous behavior. Additional experiments were also conducted by Hanes and Inman[10] using a concentric cylinder geometry with rotating side and bottom surfaces. In their work, they used non-neutrally buoyant particles (1 to 2 mm diameter) at solid fractions greater than 49%. Their results demonstrated that the shear stress depended on the shear rate to a power greater than one as the Reynolds number is increased.

A challenge that is encountered with inertial suspensions is that the experimental design may influence the measurements of the stresses. For example in a flow with rotation, the radial inertia can induce a radial velocity within the flow.[13,14] At low Reynolds number, the viscosity can suppress this radial motion, but, as the Reynolds number increases, secondary flows, often referred to as Taylor vortices, may change the character of the flow field from a simple shear flow; this change in flow character can affect the measurement of the stresses. A detailed analysis by Hunt *et al.*[15] demonstrated that Bagnold's experimental results were marred by the presence of secondary flows that developed at the boundaries of the rheometric device. By accounting for the contribution of the vortices to the shear stress, Hunt *et al.* demonstrated that Bagnold's linear to quadratic transition could be explained by assuming a laminar Newtonian flow with an effective viscosity that depended on the solid concentration. As described in the next section, the experimental measurements by Savage and McKeon were also affected by Taylor vortices.

From prior rheological studies, there is not a clear indication as to when particle collisions become important in a flow. However, the mechanics of particle collisions in a liquid have been studied for single particle-wall collisions and for binary particle collisions.[16–20] These experimental

studies measure the effective coefficient of restitution, e, defined as the ratio of rebound velocity to impact velocity, for a range of particle impact conditions and liquid properties. The coefficient of restitution is found to depend strongly on the Stokes number, which is defined as the ratio of the particle inertia to the particle drag for Stokes flow, $St = mu/(6\pi\mu a^2)$ using m as the particle mass, u as the particle velocity, and a as the particle radius. For St less than a critical value around 10, there is no rebound of the particle after impact and $e = 0$. Under these conditions, the kinetic energy of the impacting particle is eliminated due to viscous dissipation as the fluid is forced out of the region between the colliding surfaces; kinetic energy may also be lost due to inelastic deformation of the solid bodies. As the Stokes number is increased above this critical value, rebound of the particle does occur and the value of e increases monotonically with Stokes number.[17–20] For $St > 2000$, the fluid becomes negligible in the collision process and the coefficient of restitution approaches the value found in dry collisions; the value depends on the impact speed and the material properties. This dependence is the same for normal and oblique collisions between pairs of identical or dissimilar spheres, as well as for sphere-wall collisions. Aguilar-Corona *et al.*[21] measured the collision frequency in a fluidized bed and found indeed, that the collisions were damped for a Stokes number smaller than 10.

The parameter, N, used by Bagnold and other researchers[8,10] to signify the transition from a viscous-dominated suspension flow to a collision-dominated flow can be rewritten in terms of the Reynolds number, $N = h(\phi)(\rho_p/\rho_f)Re$, and the Stokes number, $N = 9h(\phi)St$, if it is assumed that the relative impact velocity of two particles colliding in a shear flow can be written as $u = \dot{\gamma}d$. The single particle coefficient of restitution studies may suggest that there is a critical Stokes number below which the collisions of the particles will be damped by the liquid (such $St < 10$) and a second value above which the viscous effects become negligible compared to the collision interactions of the particles ($St > 2000$).

The present investigation explores the rheology of an inertial suspension under conditions in which collisions may become important. The experiments use a Couette concentric cylinder rheometer designed to reduce the effect of Taylor vortices to measure the torque and shear stress on mixtures of neutrally and slightly non-neutrally buoyant particles in a Newtonian fluid. The results are presented for Reynolds numbers between 20 and 800 and Stokes numbers from 3 to 90. The present work also includes measurements for both smooth and rough walls and examines the effect of wall slip in determining the relative viscosities of the suspensions.

II. EXPERIMENTS ON INERTIAL SUSPENSIONS

A. Current experiments

The current experiments are designed to examine the effect of solid fraction and Stokes number (and equivalently the Reynolds number), at shear rates sufficiently high so particle interactions were expected to become important. Neutrally and slightly non-neutrally buoyant particles were used (ρ_p/ρ_f goes from 1.000 to 1.009). The experiments are performed for smooth and rough walls. The coaxial shear cell used in the present experiments is shown in Fig. 1. The flow is driven by the rotation of the outer cylinder. The inner cylinder consists of three sections: the rigid top and bottom sections and a central, floating section that deflects rotationally to allow measurement of the shear stress. The floating cylinder height, H, is 11.22 cm, the inner radius of the annulus, r_i, is 15.89 cm, the outer radius of the annulus, r_o, is 19.05 cm, and the width of the annulus between the cylinders, b, is 3.16 cm. The floating cylinder is supported by a central axle and knife-edge gaps (0.7 mm) that allow the floating cylinder to rotate freely while preventing particles from leaving the annular region. A seal around the axle and seals above and below the annular gap prevent the fluid from entering the bearings.

The device was specifically designed to reduce the effect of secondary vortices on the fluid measurements. The annulus height is large compared to the annular gap width (here $H/b = 11.7$; in Bagnold's experiments $H/b = 4.6$) to delay the onset of vortices. Further delay is achieved through the increase in the ratio of gap width to outer radius (b/r_o). By using the gap Reynolds number ($Re_b = \rho r_o \omega b/\mu$, where ω is the angular velocity of the outer cylinder), it is possible to determine the critical Re_b at which these secondary flows occur (Taylor[13,14]). Using the data of Taylor, a critical gap Reynolds number of 1.6×10^4 is found for this apparatus. The gap Reynolds number

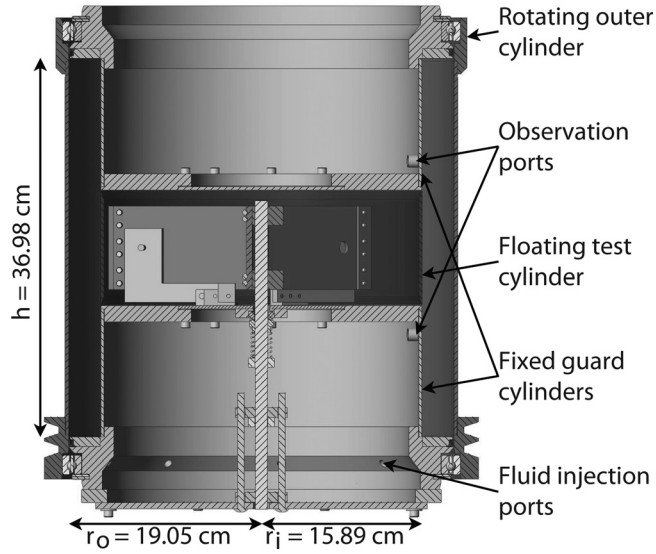

FIG. 1. Coaxial rotating cylinder, Couette flow device.

range for the current experiments is $1.2 \times 10^3 - 5.6 \times 10^4$; thus some of the experiments are above the critical Reynolds number; however, the torque measurements are taken on the floating cylinder which is some distance removed from the vortices that form as a result of the corner flow near the end plates.

The outer cylinder is driven by a belt connected to a motor; the maximum rotational speed is $\omega = 20\ \mathrm{s}^{-1}$. Hence, the maximum shear rate, $\dot{\gamma} = 2\omega r_o^2/(r_o^2 - r_i^2)$, is $110\ \mathrm{s}^{-1}$. The torque is measured by monitoring the displacement of a target attached to the floating cylinder. This displacement is opposed by a linear spring; different springs were used for different volume fractions. The deflection of the floating inner cylinder is measured using an optical probe and fotonic sensor (MTI 0623H and MTI KD-300, respectively). All torque measurements were taken several minutes after the onset of the shearing motion and averaged over an extended time. Prior to the suspension studies, tests with aqueous-glycerine mixture and no particles were run to test the experimental method. The shear stress measurements compared favorably with the theoretical results for Couette laminar flow for Reynolds numbers up to 6×10^3. The calibration data showed a maximum deviation from the theoretical Couette flow solution of 20% with the largest deviation at the lowest shear rates corresponding to the largest uncertainty in the torque measurement. The interstitial fluid temperature was measured, and the fluid properties were based on that temperature. Further details may be found in the thesis by Koos.[22]

In the present paper, the results for nylon, polystyrene, and styrene acrylonitrile particles are described. The particles differed in size, shape, and density (see Table I) and were suspended in an aqueous glycerine solution that had a density within 0.9% of the particle density. The polystyrene particles were elliptical cylinders with smooth sides. The nylon particles were nearly spherical and about twice the size of the polystyrene ones. The styrene acrylonitrile particles were ellipsoids with a diameter close to the polystyrene particles. The size of the particles used in this work is limited by the knife-edge gaps that allow the free rotation of the floating cylinder. The random loose packing ϕ_l (RLP) and the random close packing ϕ_c (RCP) of each type of particle were measured in a rectangular container with a width equal to the gap in the concentric cylinder rheometer.

To evaluate the velocities of the particles next to the inner cylinder, a pair of MTI fiber-optic proximity probes were installed flush with the surface of the inner cylinder at an observation port 2.86 cm below the floating test cylinder. These were used to both count the particles passing the probe and, by cross-correlation, to measure the velocity of those particles. The cross correlation is done over a full ten seconds to find the mean particle velocity and the measurement of individual particle velocities. The measured velocities are described in Sec. IV A.

B. Prior experiments

As described in the Introduction, there are several prior studies whose results are compared with the results of the current study. The range of experimental parameters for the current study and those earlier studies are summarized in Table II.

Similar to the current experimental design, Bagnold's experiment involved a concentric cylinder device with a fixed inner cylinder. However, three surfaces within the Bagnold apparatus rotated, and torque measurements included contributions from the flow within the gap and radial outward flow along the upper and lower plates. The overall height of the apparatus was also relatively small compared to the gap size, $H/b = 4.6$. The critical Reynolds number for the onset of Taylor vortices in Bagnold's apparatus was approximately 18 000, well below the maximum operating Reynolds number of 33 000. Chen and Ling[23] also found that the higher volume fractions tested by Bagnold ($\phi = 0.606$ and $\phi = 0.623$) were inconsistent with the lower volume fraction data. They hypothesized that this was due to the increase in particle slip against the cylinder walls. Thus, only a portion of Bagnold's data namely the data for a $Re_{gap} < 6{,}000$ is compared with the experimental results in this paper.

The experiments of Savage and McKeown[8] used an inner rotating concentric cylinder device in which the rotation induces a radial flow at a lower Reynolds number of approximately $Re_b = 200$.[24] The shear stress versus shear rate curve obtained with fluid alone was not linear, indicating the presence of Taylor vortices. The gap Reynolds number range for these experiments ($Re_b = 1{,}478 - 20{,}957$) was such that the flow was always turbulent. Because of the uncertainty of the effect of the secondary flows, the data of Savage and McKeown[8] are omitted from the comparisons of effective viscosity in this paper.

The experiments of Hanes and Inman[10] were conducted in an annular configuration in which the sides and bottom rotated. The top did not rotate and was allowed to displace upwards in response to the normal stress generated by the mixture. They examined a narrow range of volume fractions between 0.49 and 0.58. The experiments used glass beads of two sizes in both water and air. The particles used were denser than the surrounding fluid. The shearing surfaces were roughened by cementing one to two grain layers of the particles. According to the authors, the rotational speeds and applied normal stresses used in these experiments were selected to ensure that the centrifugal stress was always much less than the normal stress. The secondary flows were small compared with the primary flow and did not affect the stress measurements.[10] The authors reported that the experiments with 1.1 mm glass spheres were not consistent and that data are suspect; therefore, in this paper, comparison is only made with the data for 1.85 mm glass spheres in water.

Using an annular gap where the bottom was allowed to rotate and the top and sides remained fixed Prasad and Kytomaa[9] measured the effective viscosity of acrylic particles in an aqueous glycerine mixture ($\rho_p/\rho_f = 1.12$). The top of this apparatus could be moved up and down to vary the volume fraction between 0.49 and 0.56. The upper and bottom walls were rough with a roughness scale of the order of the particle diameter. Their results show no evidence of secondary flows present ($Re_b = 9.3 - 328$).

TABLE I. Particle properties.

	Nylon	Polystyrene	SAN[a]
Diameter (mm)	6.36	3.34	3.22
Diameter/gap width	0.2013	0.1057	0.1019
Density (kg/m^3)	1150	1050	1070
Shape	Spheres	Elliptical cylinders	Ellipsoids
Sphericity, ψ (min./max. width)	0.9999	0.7571	0.9798
RLP, ϕ_l[b]	0.568	0.553	0.611
RCP, ϕ_c	0.627	0.663	0.657

[a]Styrene acrylonitrile.
[b]The random loose and close packing (RLP and RCP) volume fractions were measured for each type of particle used in the present experiments.

In addition, the current results are compared with measurements of the effective viscosity for non-inertial flows. Zarraga *et al.*[25] studied the total stress of concentrated non-Brownian suspensions of spheres (43 μm glass beads) in Newtonian fluids. Using a parallel plate viscometer, they measured the relative viscosity which was found to be in good agreement with an empirical model proposed in their work:

$$\mu_{app}/\mu = \frac{\exp(-2.34\phi)}{(1-\phi/\phi_c)^3} \tag{1}$$

where ϕ_c is the random close packing, which corresponds to $\phi_c = 62\%$ for the particles used in their experiments. Their empirical model is in good agreement with other non-Brownian suspensions[26–28] for a Reynolds number range of 1×10^{-6} to 3×10^{-2}.

Since the experiments of Hanes and Inman[10] and Prasad and Kytomaa[9] were performed using rough walls, their data are compared with the rough walls experiments of the present work. The conditions of these non-Brownian shear flow experiments are summarized in the Table II.

III. SMOOTH WALL MEASUREMENTS

The torque measurements with polystyrene particles for volume fractions from 0.077 to 0.64 are shown in Fig. 2. Each point represents the mean of at least five individually recorded measurements; the error bars represent the standard deviation in these measurements. Linear fits for each volume fraction are also shown. As expected, the torque increases rapidly with the volume fraction, varying by several orders of magnitude between the smallest and largest volume fraction. The dependence on the volume fraction appears to be somewhat more pronounced as the volume fraction increases. The nearly linear increase in the torque with the Stokes number (and equivalently the Reynolds number for the neutrally buoyant particles, $St = \frac{1}{9}Re$) implies that the flow is close to Newtonian.

The most instructive first step in analyzing the data is to plot the ratio of the measured torque to the theoretical Couette laminar flow torque for the suspending liquid alone, which is $M_{fluid} = 4\pi\mu H\Omega r_i^2 r_o^2/(r_o^2 - r_i^2)$. Assuming that the velocity distribution of the interstitial fluid is unchanged by the presence of the particles and that the only contribution to the torque is the result of stresses from the fluid and solid phases; the ratio of the torques, M/M_{fluid}, is equal to the relative

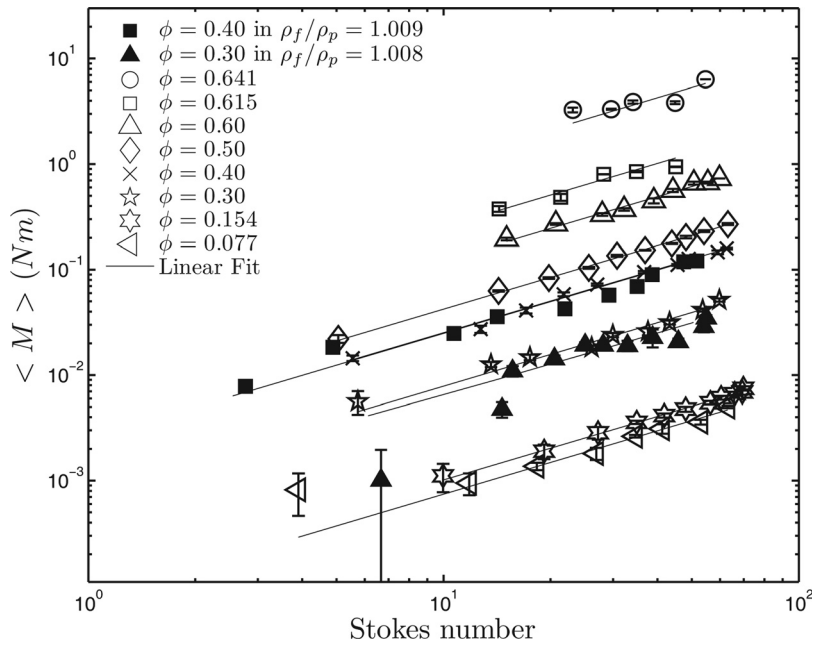

FIG. 2. The mean measured torque ($\langle M \rangle$) for suspensions of polystyrene particles in aqueous glycerine as a function of Stokes number. Closed symbols correspond to non-neutrally buoyant particles.

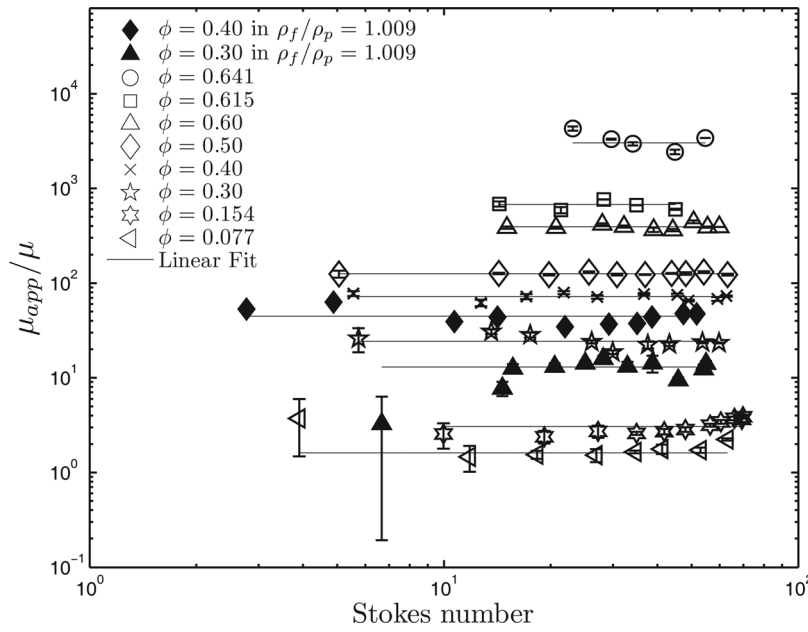

FIG. 3. The ratio of measured to pure fluid torque (μ_{app}/μ) for suspensions of polystyrene particles in aqueous glycerine. Closed symbols correspond to non-neutrally buoyant particles.

apparent viscosity μ_{app}/μ. Figure 3 presents this ratio which is a strong function of the volume fraction and relatively independent of the Stokes number (and equivalently the Re number), except at the two lowest volume fractions ($\phi = 0.077$ and $\phi = 0.154$) where the ratio of the torques exhibits an increase at the highest Stokes number. The relative apparent viscosity for the non-neutrally buoyant experiments is lower than the neutrally buoyant experiments with the same volume fraction ($\phi = 0.30$ and $\phi = 0.40$). For the non-neutrally buoyant experiments, the particles tended to float away from the central cylinder where the measurements are taken. Therefore, the actual volume fraction in the test zone may be less than the measured one. A decrease in the volume fraction would lead to a decrease in the apparent relative viscosity, which explains why the non-neutrally buoyant experiments exhibit a lower relative apparent viscosity.

If the variation in the relative apparent viscosity data is considered as a function of a modified gap Reynolds number, $\mathrm{Re}_{\mathrm{b,app}} = \rho\omega r_o b/\mu_{app}$, as in Fig. 4, the increase in the deviation from the mean value at the highest values of $Re_{b,app}$ is observed. The increases begin above a modified gap Reynolds number of about 10^4. As described in Sec. II, the onset of Taylor-Couette vortices in the present apparatus is expected to occur about $\mathrm{Re}_{\mathrm{b,app}} \approx 1.5 \times 10^4$ provided that Taylor's results[13,14] can be applied to the suspension, and the apparent viscosity of the mixture is used when calculating the Reynolds number. The increase in the apparent viscosity at the highest volume fractions in Fig. 4 may reflect the onset of these secondary flows.

At high volume fractions and the lowest $Re_{b,app}$, the normalized viscosity also deviates from one. Under these conditions, the particles may stick and slip against the inner cylinder creating a ratio of torques that is more variable than at lower volume fractions. It is possible that for such high volume fractions, the suspension regime changes to a frictional regime as classified by Coussot and Ancey,[29] where there are sustained contacts between particles.

Experiments were also performed using nylon and styrene acrylonitrile particles (see Table I) in aqueous glycerine mixtures that matched the density of the particles. The relative apparent viscosities measured for these particles are shown in Fig. 5. The relative apparent viscosity for these experiments is also a function of the volume fraction and independent of the Stokes number except at the highest solid fraction. To compare the three experiments, the volume fraction is normalized by the random loose packing ϕ_l of each type of particles. The random lose packing volume fraction was the most suitable for normalizing the volume fraction. By fitting horizontal lines to the data in Figs. 3 and 5, the dependence of μ_{app}/μ on the volume fraction is obtained as shown in Fig. 6. The data in Fig. 6 are plotted against the normalized volume fraction, ϕ/ϕ_l, to demonstrate that, despite

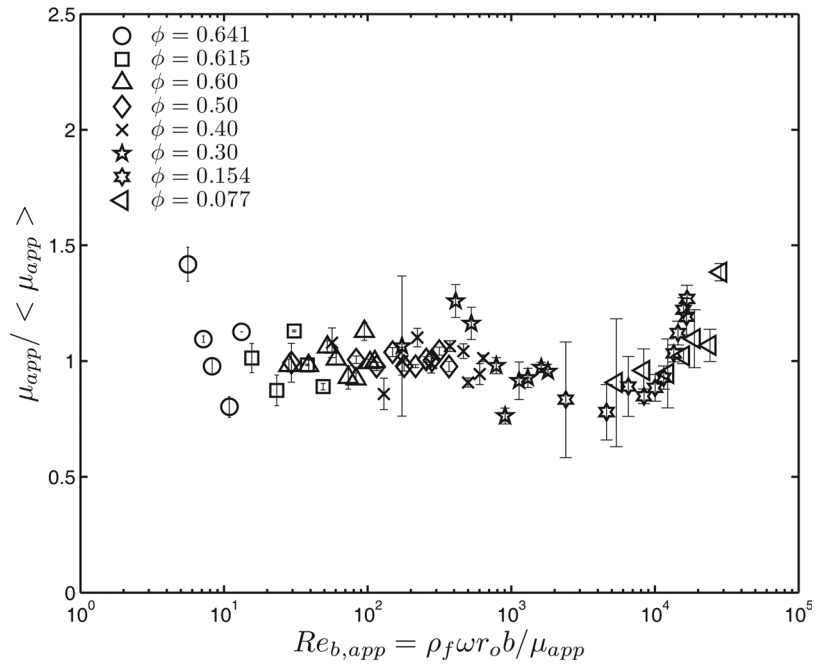

FIG. 4. Apparent viscosity divided by its mean value for neutrally buoyant polystyrene particles in aqueous glycerine solutions as a function of the modified gap Reynolds number.

differences in the particle sizes and shapes, the data for all the tested particles fall along a single curve, which correlates with the volume fraction ratio. For $\phi < \phi_l$, the curve is represented by

$$\mu_{app}/\mu = \exp\left(5.34\frac{\phi}{\phi_l}\right), \quad \phi < \phi_l. \tag{2}$$

as shown by the straight line in Fig. 6. For $\phi > \phi_l$, particle jamming occurs and the relative apparent viscosity grows more quickly than this exponential. As ϕ/ϕ_l nears unity, the number of particle collisions greatly increase. When $\phi > \phi_l$, the particles are not able to move past each other without deforming, which further increases the apparent viscosity. The influence of the particles shape on the bulk viscosity has been studied for low Re number suspensions.[30–32] These studies showed that the more the shape of the particle deviated from that of a sphere, the greater was the bulk viscosity. Moreover, aspherical particles demonstrate increased ordering near the walls (an effect which is more pronounced for the smooth walls).[33,34] The smooth wall experiments, however, show that when normalized by the size and shape dependent random loose packing fraction, ϕ_l, the relative apparent viscosity shows no dependence on the particle size or shape. Comparing the nylon to SAN particles, both have a high sphericity ($\psi = 1.00$ and 0.98), but the nylon particles

TABLE II. Previous experiments on non-Brownian shear flows.

Experiment	D (mm)	Re	St	ρ_p/ρ	Type of Rheometer
Bagnold (Refs. 7 and 11) 50% paraffin wax and lead stearate	1.32	2 - 434	0.2 - 48	1	Concentric cylinders, inner, top, and bottom rotating
Hanes *et al*. (Ref. 10) glass beads	1.85	118 - 434	36 - 134	2.8	Annular gap, inner, outer, and bottom rotating
Prasad *et al*. (Ref. 9) acrylic	3.18	0.1 - 3	0.01 - 0.4	1.12	Annular gap, bottom rotating
Present work polystyrene	3.34	25-626	3-70	1-1.009	Concentric cylinders, outer rotating
SAN[a]	3.22	25-586	3-65	1-1.002	
Nylon	6.36	55-781	6-88	1-1.003	

[a] Styrene acrylonitrile.

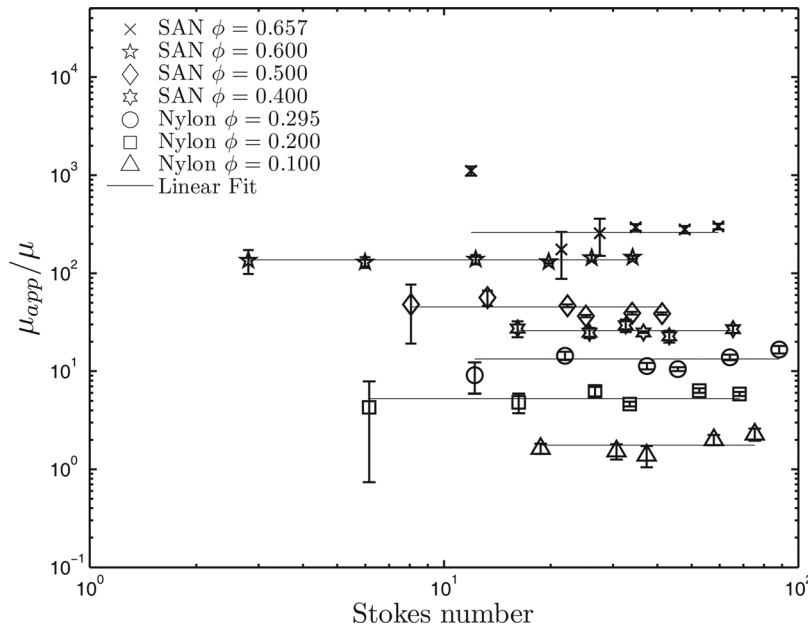

FIG. 5. The ratio of measured to pure torque for neutrally buoyant suspensions of styrene acrylonitrile and nylon particles in aqueous glycerine.

are nearly twice the size of the SAN particles. Comparing the rod-shaped polystyrene particles to the nearly spherical SAN particles, there is also no difference in the measured effective viscosity.

The present results are also compared with previous experiments of Bagnold [7,11] that were free of secondary flows ($Re_b < 6000$). These comparisons are also shown in Fig. 6. The macro-viscous data from Bagnold[7,11] compare favorably with the current experiments and shows a similar transition at ϕ_l.

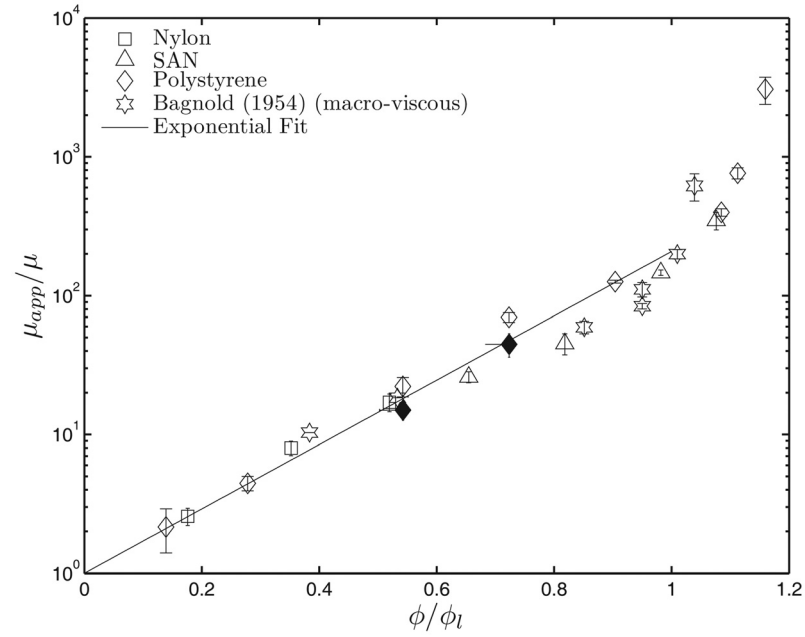

FIG. 6. Apparent viscosity ratio for different particles in aqueous glycerine. Closed symbols correspond to non-neutrally buoyant polystyrene particles. The line is an exponential fit to the data in the region, $\phi/\phi_l < 1$.

A. Rough wall experiments

Among the factors that influence the results described above is the particular structure of the liquid-solid flow at the walls of the apparatus, namely the reduction in the volume fraction near the wall and the apparent particle slip associated with that less concentrated layer. This slip is most apparent with smooth walls;[35,36] it may lead to an erroneous mixture viscosity if a correction is not applied.[3] Experiments have shown that the slip is significantly reduced when the surface roughness is the same size as or larger than the diameter of the particles.[3] To further investigate the influence of slip on the mixture viscosity measurements, additional experiments were performed with polystyrene particles. The inner and outer cylinder walls were roughened by coating them with the same polystyrene particles. The particles were glued to thin rubber sheets, which were then attached to both surfaces. The glued particles were oriented randomly and had a surface area fraction of 0.70. The decrease in gap thickness due to the rough walls was considered when calculating the shear rate for these experiments.

In the present tests with rough walls, experiments were conducted for volume fractions from 0.10 to 0.60. For each volume fraction, the measured torques were nearly a linear function of the Stokes number as in the case of the smooth wall data. Torque measurements were then normalized by the results for pure fluid torque and the resulting normalized torque measurements (equivalent to the relative effective viscosity ratio μ'/μ) are presented in Fig. 7. The effective viscosity ratio increases by almost four orders of magnitude between the lowest volume fraction and the highest volume fraction. This large increase is similar to that in the smooth wall experiments.

The mean effective viscosity ratios corresponding to the horizontal lines in Fig. 7 are plotted against the volume fraction in Fig. 8 and compared with the smooth wall data. The large increases in the relative apparent viscosity above ϕ_l that were present in the smooth wall experiments (Fig. 6) are not present in the rough wall data and, therefore, appear to be an artifact of the wall slip and depletion layers, as described in Sec. IV. The rough wall data correlate with the volume fraction ratio and, for $\phi < \phi_l$, conform to

$$\mu'/\mu = \exp\left(8.73\frac{\phi}{\phi_l}\right), \quad \phi < \phi_l. \tag{3}$$

In Figure 8, comparison is made with the data of Hanes and Inman,[10] Prasad and Kytomaa,[9] and the empirical formula of Zarraga *et al.*[25] The effective viscosities from Hanes *et al.* and Prasad

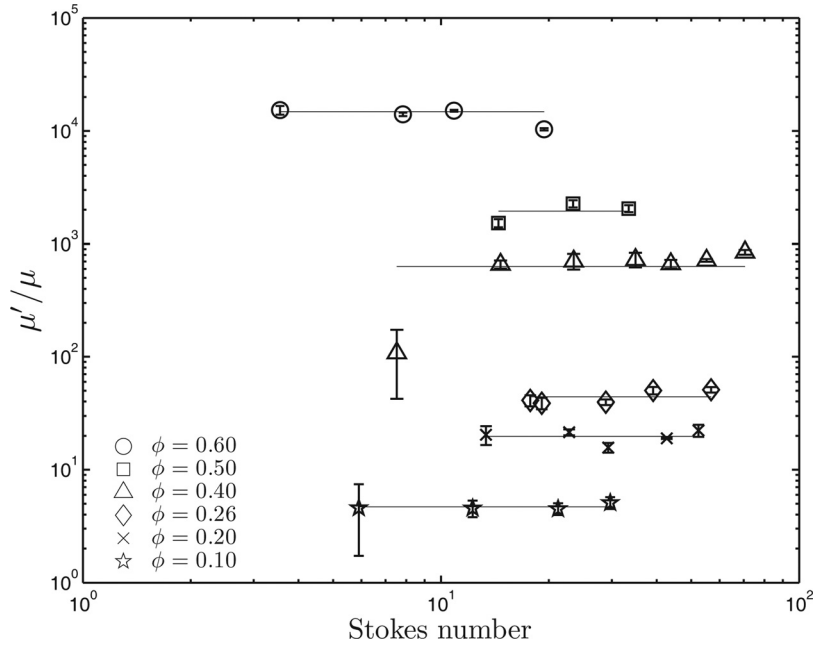

FIG. 7. Ratio of measured torque to pure fluid torque for suspensions of polystyrene particles with rough cylinder walls. The horizontal lines are fits to the data and represent the value of the ratio of effective viscosity to pure fluid viscosity μ'/μ.

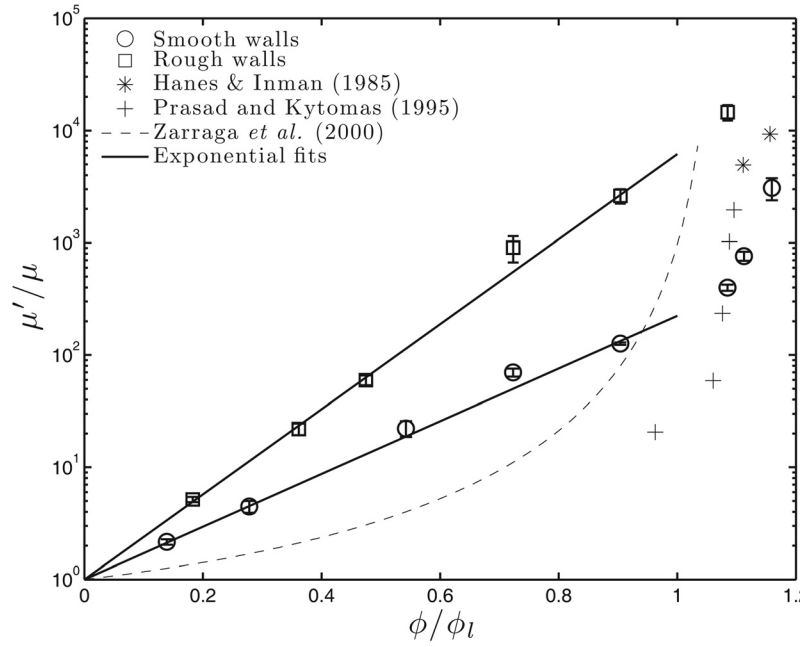

FIG. 8. Effective viscosity ratio for neutrally buoyant polystyrene particles in aqueous glycerine solutions with rough cylinder walls. The black line is an exponential fit for the points below ϕ_l.

et al. were obtained for the ratio of measured torque reported in their work and the theoretical interstitial fluid torque; their data exhibit a smaller relative effective viscosity than the current rough walls experiments. However, their experiments used non-neutrally buoyant particles; in addition, the torque was measured on the top surface of their annular gap. Hence, the torque measurements may have been affected by the migration and settling of the particles away from the top surface of the experiments. Nevertheless, the relative effective viscosities from Hanes and Inman are close to the present data. The shear rates used in their experiments were higher than those used by Prasad and Kytomaa, which may have caused a better fluidization of the suspension.

The model of Zarraga *et al*.[25] does not fit the present data. The particles used in their experiments are much smaller (of the order of microns) and, therefore, correspond to much lower Reynolds number ($Re = 1 \times 10^{-6} - 3 \times 10^{-2}$ (Refs. 26–28)). The apparent difference in relative effective viscosities may be due to a difference in the flow regime for this lower range of Reynolds numbers. Since particle interactions increase with Reynolds number and such interactions may cause mixing in the fluid, this could lead to an increase in the viscosity.

IV. SLIP AND ROUGH WALLS EXPERIMENTS

Though the interstitial fluid does not violate the no-slip condition at a solid wall, the solid particles may roll and slide, creating an effective slip.[37] Slip is composed of two components. In the first component, "true slip," solid particles are able to slide over stationary walls with a non-zero velocity creating a particle slip velocity, which is often present in granular flows[38] and more marked in densely packed flows ($\phi > \phi_l$). The second component of slip, "apparent slip," is caused by the lower concentration of particles close to the walls, resulting in a lower effective local viscosity and a higher velocity gradient. The decrease in volume fraction near the wall can be modelled by incorporating a thin depletion layer of thickness δ next to the wall in which particles are not present. This model assumes that the viscosity is uniform in both the depletion layer and the bulk core region and proceeds as follows. First note that the shear stress at the inner cylinder is given by

$$\tau_i = \mu_{app} 2\omega \frac{r_o^2}{(r_o^2 - r_i^2)}, \tag{4}$$

where μ_{app} is the apparent viscosity of the mixture (calculated from the measured torques with smooth walls). Assuming a thin inner depletion layer devoid of particles in which the shear rate is $\dot{\gamma}_i$, it also follows that $\tau_i = \mu\dot{\gamma}_i$. Consequently, the apparent viscosity can be related to the viscosity of the two phase mixture, μ' (which is assumed to be equal to the effective viscosity measured with rough walls),

$$\mu_{app} = \frac{\mu'}{2a\left(\frac{\mu'}{\mu} - 1\right) + 1}, \tag{5}$$

where a is a function of the depletion layer thicknesses, δ_i and δ_o on the inner and outer walls, respectively (see Appendix A for derivation):

$$a = \frac{\left(\frac{\delta_i}{b} r_o^3 + \frac{\delta_o}{b} r_i^3\right)}{r_o r_i (r_o + r_i)}. \tag{6}$$

Previous investigations have shown that the depletion layer thickness is generally smaller than one particle diameter; its thickness increases linearly with particle diameter and, at the same volume fraction, increases linearly with the shear stress.[39] While these depletion layers may be smaller than a particle diameter, they can significantly change the apparent viscosity.[3] In addition, the radial force in a cylindrical geometry due to differences in fluid and particle densities may accentuate the depletion layer on the inner or outer cylinder surfaces. At large volume fractions, experimentalists have found that the slip on the outer cylinder wall is negligible and that roughening the inner cylinder is sufficient to reduce the slip at the inner wall.[6,38] Direct measurements of either the slip layer thickness or measurements of both the actual and apparent viscosities are needed to quantify this error as described later in this section.

Using the values of the smooth (apparent) and the rough (effective) viscosity data of Fig. 8, the function a and the depletion layer thickness can be calculated for each volume fraction. In Fig. 9, the depletion layer thicknesses are plotted assuming that slip occurs either on the inner

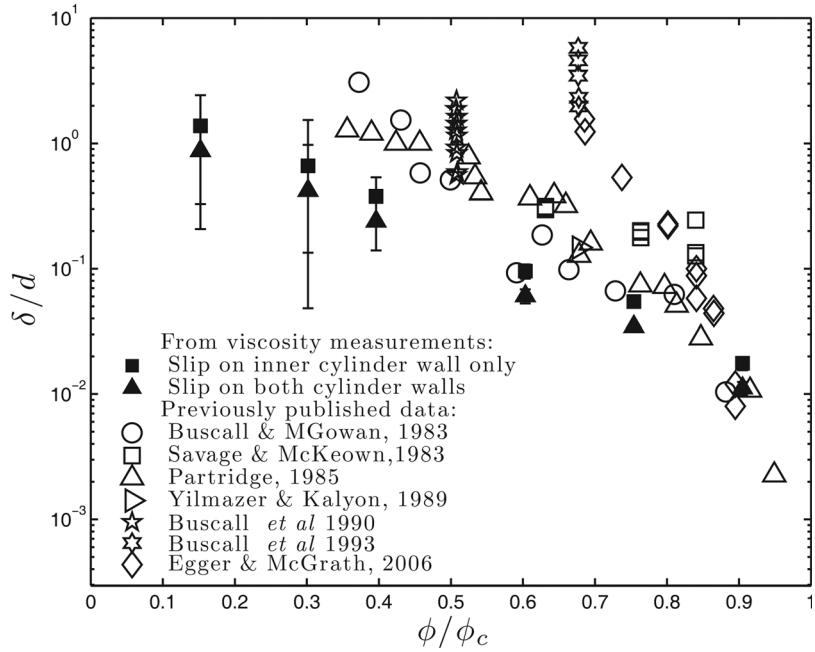

FIG. 9. Depletion layer thicknesses (divided by the particle diameter) calculated from apparent and effective viscosity measurements using Eq. 5 (closed symbols) as a function of the volume fraction ratio ϕ/ϕ_c, where ϕ_c is the random close packing. The error bars accounts for the standard deviation in the torque measurements. Also shown, typical depletion layer thicknesses on the inner cylinder of concentric cylinder devices from Refs. 6, 8, 35, 40, 41, 42, and 43 (open symbols).

cylinder alone or that the depletion thicknesses are the same on both the inner and outer cylinders. Typical depletion layer thicknesses derived from previously reported data are also shown in Fig. 9. The random close packing was used to normalized the volume fraction. Even though the data from Savage and McKeown[8] were not used for comparison of the effective viscosity, their shear stress measurements with smooth and rough wall were used to calculate the depletion layer thickness by using Eq. (5) and assuming slip on the inner cylinder only. Their data are used for this comparison because the particles used in their experiments (polystyrene beads $d \approx 1$ mm) are approximately the same size as used in the present experiments. Egger and McGrath data for a $d \approx 0.5$ μm emulsion were obtained considering slip on both cylinders and following a different approach described by the authors[43] and discussed later in this section. The rest of the data in Fig. 9 were calculated from shear stress measurements for $d \approx 1$ μm polystyrene beads as reported in Buscall *et al.*[6] and considered slip only on the inner cylinder. The calculated depletion layer thickness is close to, though slightly less than, previously recorded data. This may due to the fact that Egger and McGrath[43] and Buscall *et al.*[6] considered a more idealized scenario. Egger and McGrath followed the approach made by Russel and Grant[44] where they assumed that the applied shear stress at a given radius is uniform over the whole sample. Egger and McGrath validated this assumption by the closeness in the mapping of their rough wall data and the slip corrected data. Buscall *et al.*[6] assumed that the actual viscosity (which they called true viscosity) is large enough so its inverse value can be neglected. With the current data, there is little difference between the predicted values using slip on the inner wall or on both walls, though the assumption of slip in the inner wall alone results in a better match to previously recorded data.

A. Slip velocity measurement

To further explore the slip effects in the present experiments, particle velocities next to the inner cylinder wall (u_w) were measured using the probes described earlier; the average and individual particle speeds were recorded. Figure 10 shows a typical distribution of these individual particle velocity fluctuations, defined as the difference between the particle velocity and its mean. The standard deviations of these distributions (normalized by the mean velocity) are plotted in Fig. 11 and, for all but the lowest velocities, the standard deviation remains a constant percentage

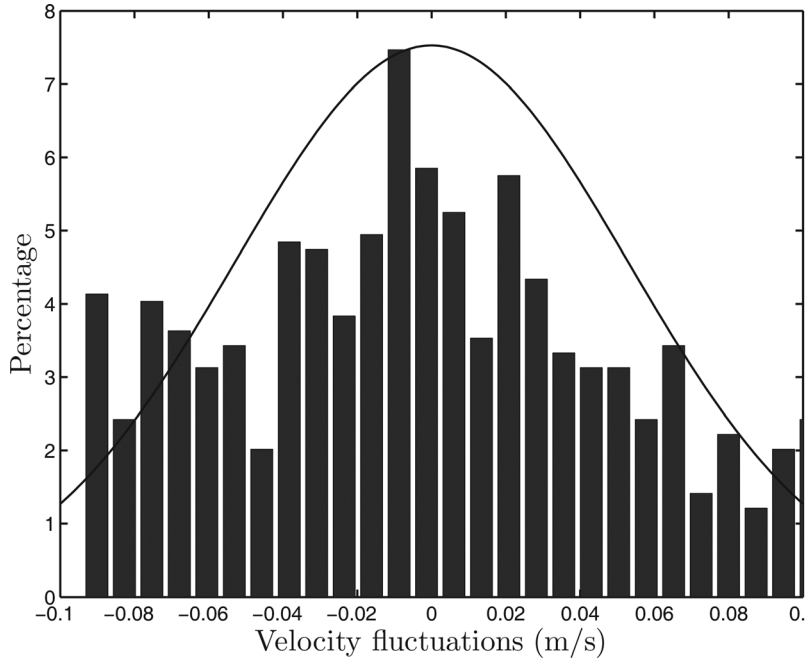

FIG. 10. A typical distribution of particle velocity fluctuations (the individual particle velocities minus the mean value $\langle u_w \rangle$) for $\phi = 0.253$ of polystyrene particles in aqueous glycerine ($\rho_f/\rho_p = 0.997$) rotating at 1.4 m/s. Also shown is a Gaussian normal distribution with a standard deviation of 0.053 m/s.

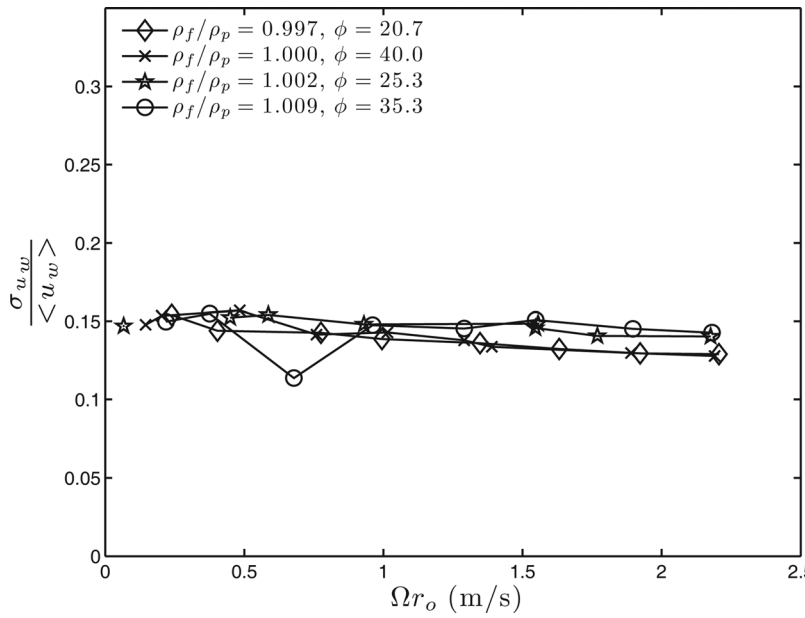

FIG. 11. Standard deviation in particle velocity (σ_{u_w}) normalized by the mean value ($\langle u_w \rangle$). With the exception of the low rotational velocity points, the spread in the particle velocities remains fairly constant.

of the mean velocity between 12% and 18%. Some of the variation may result from the velocity gradient near the wall; for example, a 0.1 - 0.5 diameter displacement in the particle distance from the wall would lead to a 20% change in the fluid velocity assuming a Couette laminar flow. Alternatively, the deviations could be due to random velocity components, a manifestation of the variation in particle trajectories due to collisions near the wall.

The depletion layer on the inner cylinder can also be estimated from the measurements of the particle velocities. By assuming that there are no particles in the depletion layer and that the particles viewed by the optical probes are those at the depletion layer-core region interface, the interfacial velocity, u, at $r = r_i + \delta_i$ is given by

$$\frac{u}{\omega r_o} = \frac{2\delta_i r_o}{r_o^2 - r_i^2}\frac{\mu_{app}}{\mu}, \tag{7}$$

(see Appendix B for derivation) and this can be used along with the measured particle velocities, u, to obtain estimates of the depletion layer thickness, δ_i. The calculated thicknesses are shown in Fig. 12 as a function of Stokes number and volume fraction. Note that the thickness is relatively independent of Stokes number but varies substantially with the volume fraction. The same data are included in Fig. 13 where it is seen to be consistent with the values derived from the present rheological measurements. Note that the present estimates for the depletion layer thickness fall slightly below previously published data for volume fraction below ϕ_l. This deviation can be explained by the ordering of particles next to the walls. Specifically, the surface area oriented towards the optic probes fluctuates as a function of the distance from the wall.[45] These fluctuations can give rise to errors in the measurements of the particle velocity. In the present experiments, the orientation of the particles should result in the depletion layer thickness being underestimated.

V. DISCUSSION AND SUMMARY

Rheological measurements of concentrated, particle-liquid mixtures in a concentric cylinder device were carried out using both smooth and rough cylinder surfaces. For the smooth walls, three different types of particles were tested. Despite differences in the particle materials, sizes, and shapes, the data for all tested particles correlate with the volume fraction ratio for $\phi < \phi_l$. A slight mismatch in the fluid and particle density (within 1%) does not change the dependency of the apparent viscosity on the volume fraction ratio ϕ/ϕ_l. In the "rough wall" experiments only one

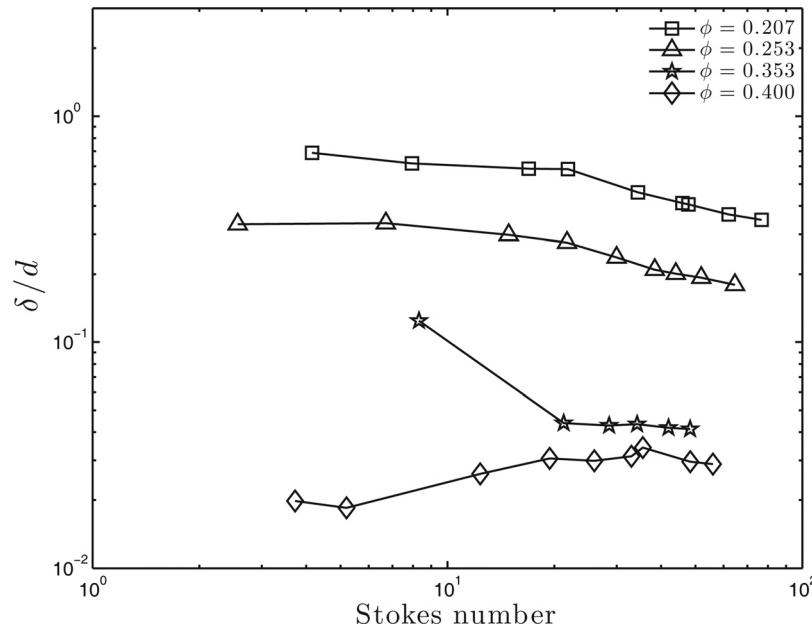

FIG. 12. Depletion layer thicknesses (δ) calculated from the particle velocity measurements as a function of Stokes number for several volume fractions.

type of particles was tested. These particles were glued to both the inner and outer cylinder walls. This configuration appears to result in appropriate effective mixture viscosities that increase exponentially with the volume fraction up to the loose packed volume fraction. On the other hand, the measurements with smooth wall cylinders clearly demonstrate that wall slip substantially affects the apparent viscosity. The slip is modelled by assuming thin depletion layers on the smooth walls. The thickness of the depletion layers were estimated by measuring the particle velocities near the walls. In addition, the values for the rough and smooth wall viscosities were used to evaluate the

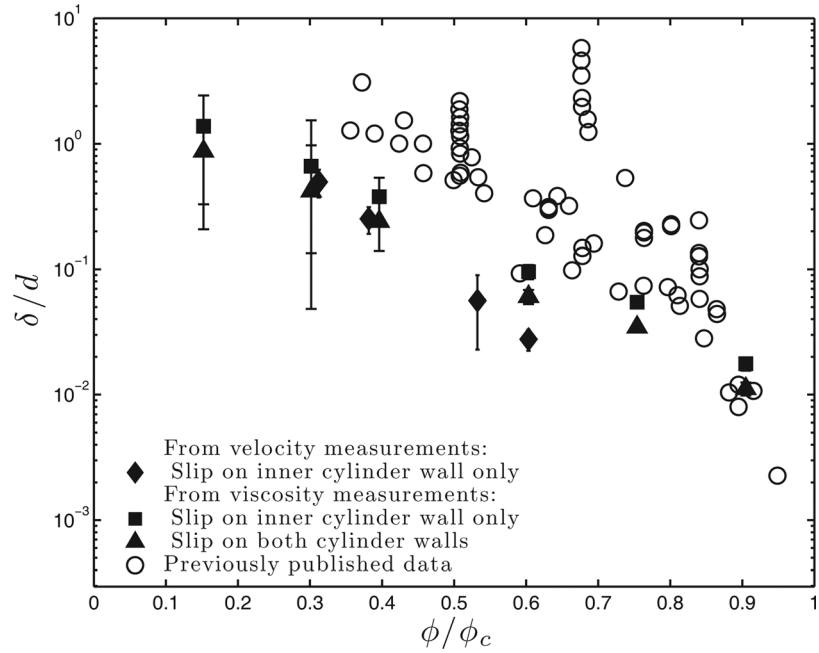

FIG. 13. Depletion layer thicknesses calculated from apparent and effective viscosity measurements using Eq. (5) and depletion thicknesses calculated from the velocity measurements using Eq. (7). Also shown are the previously reported experimental values from Fig. 9.

thickness of the depletion layer over the full range of volume fractions. From these two methods, the resulting depletion layer thicknesses are shown to be in agreement with previous investigations. For volume fractions less than the loose packed volume fraction, ϕ_l, the slip is caused by thin depletion layers that decrease in thickness as the volume fraction is increased. For $\phi > \phi_l$, slip caused by particles sliding over the cylinder walls appears to dominate and contributes significantly to the differences between the smooth and rough wall measurements.

The initial motivation of the current study was to examine the effects of particle collisions on the shear stress for an inertial suspension. It was expected that given the range of $\dot{\gamma}$ used (1-100 s^{-1}), the regime of the suspension would be dominated by inertia. In such regime, it is hypothesized that the direct particle-particle collision is the dominant mechanism of transporting momentum and energy. Therefore, stresses scale inertially and are proportionally to the shear rate to a power larger than one. However, the current torque measurements for rough and smooth walls scale linearly with the shear rate. Based on the previous studies of the coefficient of restitution of immersed sphere collisions, our data are far from the regime where the particle collisions become important. The range of Stokes numbers used in the present work is such that the particle interactions are damped due to viscous dissipation of the interstitial fluid. Still the measured relative viscosities are higher than the previous experiments, which may results from the induced mixing of the fluid due to particle interactions.

ACKNOWLEDGMENTS

This research was supported by NASA grant NNC04GA48G, NSF grant 0730284, and through the generous support of the Roberto Rocca Education Program for ELG.

APPENDIX A: APPARENT VISCOSITY

The velocity field in a rotational coaxial cylinder rheometer for a Newtonian fluid is given by[46]

$$u = c_1 r + \frac{c_2}{r}.$$

The flow of a suspension in a rheometer with smooth walls will present a thin layer of fluid near the walls. Thus, the coaxial cylinder Couette flow with slip can be modeled as three regions flow: two thin layers composed of only liquid next to the rheometer walls and a core region composed of liquid and particles where both, the depletion layer and core region, are treated as Newtonian. The velocity field in each region can be written as:

$$\begin{aligned} u(r) &= c_1 r + \frac{c_2}{r}, r_i \le r \le r_i + \delta_i, \\ u(r) &= c_3 r + \frac{c_4}{r}, r_i + \delta_i \le r \le r_o - \delta_o, \\ u(r) &= c_5 r + \frac{c_6}{r}, r_o - \delta_o \le r \le r_o, \end{aligned}$$

where δ_i and δ_o are the depletion layer thickness for the inner and outer wall, respectively. The no slip at the wall condition holds since the depletion layers are considered to be composed of only liquid. It is also assumed that the shear stress is continuous at the depletion layer-core region interface. These assumptions result in 6 boundary conditions that lead to the following system of equations:

$$\begin{aligned} c_1 r_i + \frac{c_2}{r_i} &= 0, \\ c_1(r_i + \delta_i) + \frac{c_2}{r_i + \delta_i} &= c_3(r_i + \delta_i) + \frac{c_4}{r_i + \delta_i}, \\ c_3(r_o - \delta_o) + \frac{c_4}{r_o - \delta_o} &= c_5(r_o - \delta_o) + \frac{c_6}{r_o - \delta_o}, \\ c_5 r_o + \frac{c_6}{r_o} &= \omega r_o, \\ \mu c_2 &= \mu' c_4, \\ \mu' c_4 &= \mu c_6, \end{aligned}$$

where μ' is the viscosity of the two-phase flow (assumed to be the viscosity measured with rough walls) and μ is the interstitial fluid viscosity. The system can be further reduced by introducing the apparent viscosity (μ_{app}) defined as the viscosity measured with smooth walls and the apparent shear rate ($\dot{\gamma}_{app} = 2\omega r_o^2/(r_o^2 - r_i^2)$) for an annular flow where the inner cylinder is stationary, the outer cylinder rotates and follows the no slip condition at the wall. Hence, the shear stress at the inner cylinder is given by $\tau_i = \mu_{app}\gamma_{app} = \mu\dot{\gamma}_i$, where $\dot{\gamma}_i$ is the shear rate at the inner wall depletion layer region. By solving the reduced system of equations, the following relation is obtained:

$$\frac{\mu}{\mu_{app}} = \frac{r_o^2 r_i^2}{r_o^2 - r_i^2}\left[\left(1 - \frac{\mu}{\mu'}\right)\left(\frac{1}{(r_o - \delta_o)^2} - \frac{1}{(r_i + \delta_i)^2}\right) + \frac{1}{r_i^2} - \frac{1}{r_o^2}\right]. \tag{A1}$$

The depletion layer thicknesses are small compared with the cylinder radii, hence by Taylor expansion

$$\frac{1}{(r_i + \delta_i)^2} \approx \frac{1}{r_i^2} - \frac{2\delta_i}{r_i^3},$$
$$\frac{1}{(r_o - \delta_o)^2} \approx \frac{1}{r_o^2} + \frac{2\delta_o}{r_o^3};$$

therefore, the ratio of fluid and apparent viscosity reduces to

$$\frac{\mu}{\mu_{app}} = \left[\left(1 - \frac{\mu}{\mu'}\right)\left(2\frac{r_o^2\frac{\delta_i}{r_i} + r_i^2\frac{\delta_o}{r_o}}{r_o^2 - r_i^2} - 1\right) + 1\right]. \tag{A2}$$

Using $a = \left(r_o^2\frac{\delta_i}{r_i} + r_i^2\frac{\delta_o}{r_o}\right)/(r_o^2 - r_i^2)$, then

$$\frac{\mu}{\mu_{app}} = (1 - \frac{\mu}{\mu'})(2a - 1) + 1. \tag{A3}$$

APPENDIX B: PARTICLE VELOCITY

The depletion layer thickness can be calculated from the velocity of the particles. Assume that the particle velocity is equal to the velocity at $r_i + \delta_i$

$$\begin{aligned} u_{particle} &= c_1(r_i + \delta_i) + \frac{c_2}{r_i + \delta_i} \\ &= -\frac{\omega r_o^2 r_i^2}{r_o^2 - r_i^2}\frac{\mu_{app}}{\mu}\left(\frac{1}{r_i + \delta_i} - \frac{r_i + \delta_i}{r_i^2}\right). \end{aligned} \tag{B1}$$

Let $x = \frac{ri}{r_o}$ and $d = \frac{\delta_i}{r_o}$

$$\therefore \frac{u_{particle}}{\omega r_o} = -\frac{r_o^3 x^2}{r_o^2 - r_o^2 x^2}\frac{\mu_{app}}{\mu}\left(\frac{1}{xr_o + dr_o} - \frac{xr_o + dr_o}{x^2 r_o^2}\right) = -\frac{x^2}{1 - x^2}\frac{\mu_{app}}{\mu}\left(\frac{1}{x + d} - \frac{x + d}{x^2}\right). \tag{B2}$$

Considering that $d \ll 1$ the velocities ratio simplifies to

$$\begin{aligned} \frac{u_{particle}}{\omega r_o} &= \frac{x^2}{1 - x^2}\frac{\mu_{app}}{\mu}\left(\frac{x + d}{x^2} - \frac{1}{x} + \frac{d}{x^2}\right) \\ &= \frac{2d}{1 - x^2}\frac{\mu_{app}}{\mu} \\ &= \frac{2\delta_i r_o}{r_o^2 - r_i^2}\frac{\mu_{app}}{\mu}. \end{aligned} \tag{B3}$$

[1]H. A. Barnes, "Shear-thickening ('Dilatancy') in suspensions of nonaggregating solid particles dispersed in Newtonian liquids," J. Rheol. **33**, 329 (1989).
[2]J. J. Stickel and R. L. Powell, "Fluid mechanics and rheology of dense suspensions," Annu. Rev. Fluid Mech. **37**, 129 (2005).
[3]H. A. Barnes, "Measuring the viscosity of large-particle (and flocculated) suspensions – a note on the necessary gap size of rotational viscometers," J. Non-Newtonian Fluid Mech. **94**, 213 (2000).
[4]R. G. Larson, *The Structure and Rheology of Complex Fluids* (Oxford University Press, New York, 1999).
[5]S. A. Khan, S. A. Schnepper, and R. C. Armstrong, "Foam rheology.3. Measurement of shear-flow properties," J. Rheol. **32**, 69 (1988).
[6]R. Buscall, I. J. McGowan, and A. J. Morton-Jones, "The rheology of concentrated dispersions of weakly attracting colloidal particles with and without wall slip," J. Rheol. **37**, 621 (1993).
[7]R. A. Bagnold, "Experiments on a gravity-free dispersion of large solid spheres in a Newtonian fluid under shear," Proc. R. Soc. London, Ser. A **225**, 49 (1954).
[8]S. B. Savage and S. McKeown, "Shear stresses developed during rapid shear of concentrated suspensions of large spherical particles between concentric cylinders," J. Fluid Mech. **127**, 453 (1983).
[9]D. Prasad and H. K. Kytomaa, "Particle stress and viscous compaction during shear of dense suspensions," Int. J. Multiphase Flow **21**, 775 (1995).
[10]D. M. Hanes and D. L. Inman, "Observations of rapidly flowing granular-fluid materials," J. Fluid Mech. **150**, 357 (1985).
[11]R. A. Bagnold, "The flow of cohesionless grains in fluids," Proc. R. Soc. London, Ser. A **249**, 235 (1956).
[12]G. Zeininger and C. E. Brennen, "Interstitial fluid effects in hopper flows of granular materials" *ASME. Cavitation and Multiphase Flow forum* (American Society of Mechanical Engineers, New York, 1985).
[13]G. I. Taylor, "Fluid friction between rotating cylinders, I. Torque measurements," Proc. R. Soc. London, Ser. A, **157**, 546 (1936).
[14]G. I. Taylor, "Fluid friction between rotating cylinders, II. Distribution of velocity between concentric cylinders when outer one is rotating and inner one is at rest," Proc. R. Soc. London, Ser. A **157**, 565 (1936).
[15]M. L. Hunt, R. Zenit, C. S. Campbell, and C. E. Brennen, "Revisiting the 1954 suspension experiments of R. A. Bagnold," J. Fluid Mech. **452**, 1 (2002).
[16]F. L.Yang and M. L. Hunt "Dynamics of particle-particle collisions in a viscous liquid," Phys. Fluids **18**, 121506 (2006).
[17]M. H. MacLaughlin "An experimental study of particle-wall collision relating to flow of solid particles in a fluid," Ph.D. Thesis (California Institute of Technology, 1968).
[18]J. M. Serayssol, R. H. Davis, and E. J. Hinch "The elastohydrodynamic collision of two spheres," J. Fluid Mech. **163**, (1986).
[19]G. G. Joseph, R. Zenit, M. L. Hunt, and A. M. Rosenwinked "Particle-wall collisions in a viscous fluid," J. Fluid Mech. **433**, 329, (2001).
[20]G. G. Joseph and M. L. Hunt "Oblique particle-wall collisions in a liquid," J. Fluid Mech. **510**, 71, (2004).
[21]A. Aguilar-Corona, R. Zenit, and O. Masbernat "Collisions in a liquid fluidized bed," Int. J. Multiphase Flow **10**, 1, (2011).
[22]E. Koos, "Rheological Measurements in Liquid-Solid Flows," Ph.D. Thesis (California Institute of Technology, 2009).
[23]C. L. Chen and C. H. Ling, "Granular-flow rheology: Role of shear-rate number in transition regime," ASCE J. Eng. Mech. **122**, 469 (1996).
[24]E. L. Koschmieder, *Bénard Cells and Taylor Vortices* (Cambridge University Press, Cambridge, 1993).
[25]I. E. Zarraga, D. A. Hill, and D. T. Leighton, Jr., "The characterization of the total stress of concentrated suspensions of noncolloidal spheres in Newtonian fluids," J. Rheol. **44**, 185 (2000).
[26]A. Acrivos, X. Fan, and R. Mauri, "On the measurements of the relative viscosity of suspensions," J. Rheol. **38**, 1285 (1994).
[27]G. Ovarlez, F. Betrand, and S. Rodts, "Local determination of the constitutive law of dense suspension of noncolloidal particles through magnetic resonance imaging," J. Rheol. **50**, 259 (2006).
[28]C. Bonnoit, T. Darnige, E. Clement, and A. Lindner, "Inclined plane rheometry of a dense granular suspension," J. Rheol. **54**, 65 (2010).
[29]P. Coussot and C. Ancey, "Rheophysical classification of concentrated suspensions and granular pastes," Phys. Rev. E **59**, 4445 (1999).
[30]B. Clarke, "Rheology of coarse settling suspensions," Trans. Inst. Chem. Eng. **45**, 6 (1967).
[31]S. G. Ward and R. L. Whitmore, "Studies of the Viscosity and Sedimentation of Suspensions. 1. The viscosity of suspension of Spherical Particles," Br. J. Appl. Phys. **1**, 286 (1950).
[32]C. Moreland, "Viscosity of Suspension of coal in mineral oil," Can. J. Chem. Eng. **41**, 24 (1963).
[33]A. Chrzanowska, P. I. C. Teixeira, H. Ehrentraut, and D. J. Cleaver, "Ordering of hard particles between hard walls," J. Phys.: Condens. Matter, **13**, 4725 (2001).
[34]T. Börzsönyi, T. C. Halsey, and R. E. Ecke, "Avalanche dynamics on a rough inclined plane," Phys. Rev. E, **78**, 11306 (2008).
[35]U. Yilmazer and D. M. Kalyon, "Slip effects in capillary and parallel disk torsional flows of highly filled suspensions," J. Rheol., **33**, 1197 (1989).
[36]S. A. Gulmus and U. Yilmazer, "Effect of the surface roughness and construction material on wall slip in the flow of concentrated suspensions," J. Appl. Polym. Sci., **103**, 3341 (2007).
[37]A. Acrivos, *The Rheology of Concentrated Suspensions of Non-Colloidal Particles* (M.C. Roco, Butterworth-Heinemann, Boston, 1992).
[38]H. A. Barnes, "A review of the slip (wall depletion) of polymer solutions, emulsions and particle suspensions in viscometers: its cause, character, and cure," J. Non-Newtonian Fluid Mech., **56**, 221 (1995).
[39]F. Soltani and U. Yilmazer, "Slip velocity and slip layer thickness in flow of concentrated suspensions," J. Appl. Polym. Sci. **70**, 515 (1998).
[40]R. Buscall and I. J. McGowan, "Sedimentation and viscous flow of a weakly flocculated concentrated dispersion -A comparative-study," Faraday Special Discuss. Chem. Soc. **76**, 277 (1983).
[41]S.J. Partridge, "The rheology of cohesive sediments," Ph.D. Thesis (University of Bristol, 1985).

[42]R. Buscall, I. J. McGowan, and C. A. Mumme-Young, "Rheology of weakly interacting colloidal particles at high concentration," Faraday Special Discuss. Chem. Soc. **90**, 115 (1990).
[43]H. Egger and K. M. McGrath,"Estimating depletion layer thickness in colloidal systems: correlation with oil-in-water emulsion coposition," Colloids Surf., A **225**, 107 (2006).
[44]W. B. Russel and M. C. Grant, "Distinguishing between dynamic yielding and wall slip in a weakly flocculated colloidal dispersion," Colloids Surf., A **171**, 271 (2000).
[45]X. Chen and M. Louge, "Heat transfer enhancement in dense suspensions of agitated solids. Part I: Theory," Int. J. Heat Mass Transfer **51**, 5108 (2008).
[46]H. Schlichting, *Boundary Layer Theory* (McGraw Hill, New York, 1951).